P2.12

NUMERICAL STUDY ON THE EXTRATROPICAL TRANSITION OF TYPHOON BART (1991) OVER THE WESTERN NORTH PACIFIC OCEAN

* Jun Yoshino, Hirohiko Ishikawa and Hiromasa Ueda

Disaster Prevention Research Institute, Kyoto University, Kyoto, Japan

1. INTRODUCTION

In recent few years, considerable concern has been raised about the extratropical transition (ET) of tropical cyclone (TC). As a TC approaches mid-latitude baroclinic zone, it would drastically change its structure and strength. Because it begins to interact with surrounding systems such as synoptic troughs, ridges and jet streams. Futhermore, once the ET of TC proceeds, the TC, characterized as the axisymmetric warm core structure, would be transformed to the extratropical cyclone, featured as the asymmetric cold core structure.

Bosart and Lackmann (1995) have examined the rapid re-development of Hurricane David (1979) in the weakly baroclinic zone from the perspective of potential vorticity (PV). They suggested that David has came under the influence of an upper tropospheric PV anomaly, resulting in the tropopause lifting due to the upper level frontogenesis and compaction of the PV maximum. Comparative study of the ET between Hurricane Felix (1995) and Hurricane Iris (1995) has been conducted using a PV thinking by Thorncroft and Jones (2000). It was found that the life-cycle of Felix was fairly different from Iris. The former combined with the predominantly northeast-southwest-oriented thin upper-trough, which life-cycle are called as the "LC1 life-cycle". The latter was characterized by its less northward shift and the cyclonic warp-up of the high PV anomaly in the upper-level trough, the so-called "LC2 life-cycle". These life-cycles appear even in the case of mid-latitudinal extratropical cyclones, as well as TCs in ET (Thorncroft et al. 1993).

Some attempts of numerical simulation have been conducted in order to investigate the detailed structure and life-cycle of TCs in ET. Ritchie and Elsberry (2001) performed the simulation of a TC in an idealized baroclinic environment, and showed the transformations of flow and cloud pattern in each stage of ET. McTaggart-Cowan et al. (2001) also conducted sensitivity simulations of the re-intensification of a mid-latitude TC event, and found that the primary role for the cyclogenesis of the TC in mid-latitude was the existence of an upstream upper-level trough, while the remnants of TC in mid-latitude was the minor contribution by comparison. Thus, considerable evidence has accumulated in recent years on the re-intensification of the ET of TCs. The comprehensive understanding about the transition from TC to extratropical cyclone, however, is still lacking. It is therefore necessary to investigate further cases of the ET of TCs.

Typhoon Bart (1999) has undergone the rapid weakening (a central pressure change of $+50$-hPa/day) around Japan Islands and the unexpected re-intensification (-15-hPa/day) over the Sea of Okhotsk in September 1999. The purpose of this study is to investigate the detailed structure and life-cycle of Bart in mid-latitude using the regional numerical climate model PSU/NCAR MM5 (Dudhia 1993). In addition to the full physics simulation, some sensitivity experiments relating to physical parameterization (i.e. latent heat release and boundary layer processes) are also conducted. Employing the gridded datasets from the successful simulation, the analysis using a piecewise PV inversion technique (developed by Davis and Emanuel (1991)) is performed, in order to determine the relatively contributions of discrete pieces of PV anomaly to the rapid decaying and re-intensification of Bart.

2. OUTLINE OF TYPHOON BART (1999)

Figure 1 shows the JMA (Japan Meteorological Agency) best track of Typhoon Bart (1999). Bart formed to the south of Okinawa Island, Japan, on 17 September 1999, and reached to typhoon strength by 0900JST 19. After its westward movement, Bart turned north-northeastward on 20 Sep. and accelerated its movement of over 20 m/s on 23 September. Bart struck Kyushu Island, west Japan, early on 24 Sep., when it brought about the severe disasters of high tide at Kumamoto Prefecture and F3 tornadic disaster at Aichi Prefecture (Yoshino et al. 2002). After that, Bart moved northeastward to the Sea of Japan with increasing its moving speed. Bart became an extratropical cyclone at 1200JST 25 September (from the definition of JMA).

Figure 2 shows time series of the minimum sea level central pressure by the JMA best track. Bart reached to a maximum intensity of 930 hPa on 22 Sep. before its landfall. After the landfall (on 24 Sep.), Bart drastically decreased its strength (+50 hPa/day) as mentioned above, and reached a minimum central

* *Corresponding author address*: Jun Yoshino, Severe Storm Research Section, Disaster Prevention Research Institute, Kyoto University, Gokasho, Uji, Kyoto Prefecture, Japan; email: yoshino@storm.dpri.kyoto-u.ac.jp

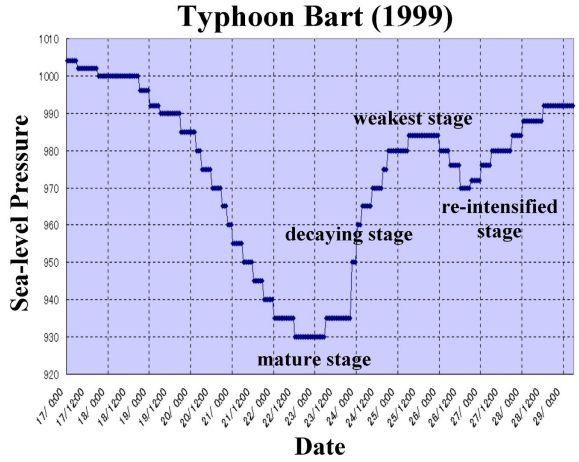

Figure 1 : Time series of the sea level central pressure of Typhoon Bart (1999) from its generation to its dissipation.

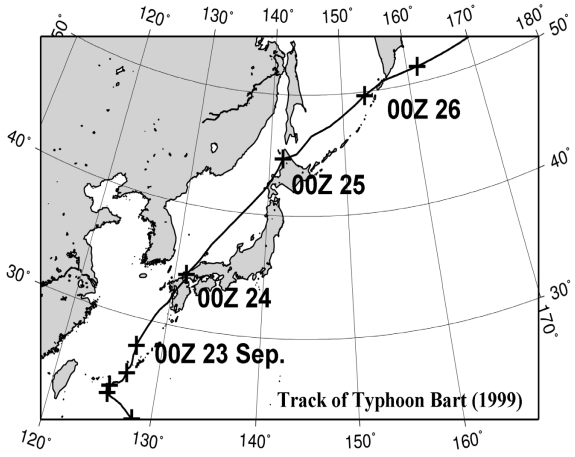

Figure 2 : Track of Typhoon Bart. Plus marks indicate typhoon position every 24-hours.

pressure of 985 hPa on 25 September. Although its intensity has been weakening for a couple of days, Bart started to change its features and to intensify its strength on 26 September. In the re-intensified stage, the minimum sea level pressure was 970 hPa at 1200JST 24. The deepening rate was -15 hPa in 12 hours (-30 hPa/day), which was categorized as a bomb (Sanders and Gyakum 1980).

Figures 3 (a) $\sim$ (d) illustrate the cloud patterns of Bart by GMS-5 infrared images. At 0000Z 24 Sep. (see Figure 3 (a)), the cloud distribution of Bart was roughly axisymmetry, and began to connect with a pre-existing front north of Bart. As Bart moved northeastward (1200Z 24), its phasis shifted the axisymmetric pattern to asymmetry as Figure 3 (b) shown. The cloud band concentrated on the north of the typhoon center. The relatively dry air, originating from the western system of Bart, is prevailing over the south of the center. When Bart came to be in the weakest stage (1500Z 25) as Figure 3 (c) shown, Bart possessed a straight west-east-oriented cloud band, which was corresponding to a warm front of the extratropical cyclone system. Although the TC activity seemed to vanish completely, Bart brought back its cyclonic activity in the re-intensification stage (1500Z 26), as Figure 3 (d) illustrated. Obviously, the re-intensified Bart rolled up the cloud bands spirally and got the axisymmetric pattern again as the mature stage. After the re-intensification, the cyclonic activity of the extratropical typhoon has disappeared over the Bering Sea.

3. MODEL DESCRIPTION

The Penn State University and National Center for Atmospheric Research Regional Climate Modeling System MM5 (Dudhia 1993) was chosen to examine the high-resolution dynamical processes of the ET of Typhoon Bart. The horizontal grid size of 30-km ($301\times250\times23$) was used for the single computational domain. Initial and boundary conditions were provided by the fourth daily NCEP global final analyses, with a resolution of 1.0 $\times$ 1.0 degree. The dataset of sea surface temperature at a resolution of 1.0 $\times$ 1.0 degree from the NCEP optimum interpolation SST analyses was employed, and held constant throughout the whole simulated period. Initial atmospheric fields were modified using the typhoon bogussing scheme (Low-Nam and Davis 2001), because the strength of the analysed typhoon was much weaker.

The MM5 simulation ran with the several physical parameterizations as the followings. The high resolution Blackadar PBL scheme was utilized to represent the planetary boundary layer physics. Surface temperature over land is calculated by the force-restore slab model. The Reisner mixed-phase scheme, which includes prognostic equations for mixing ratio of water vapor, cloud water, rain, cloud ice, snow, graupel, and ice number, was employed as the processes of explicit microphysics. The Grell cumulus parameterization scheme was simultaneously operating for consideration of subgrid-scale cloud properties. The model also used the longwave and shortwave radiation scheme that mutually interact with the clear sky, clouds, precipitation, and gourd. The simulation was initialized from 0000Z 21 Sep. and run out to 162-hours.

4. PIECEWISE POTENTIAL VORTICITY INVERSION

The piecewise PV inversion technique developed by Davis and Emanuel (1991) was used for evaluations of the balanced fields associated with each PV

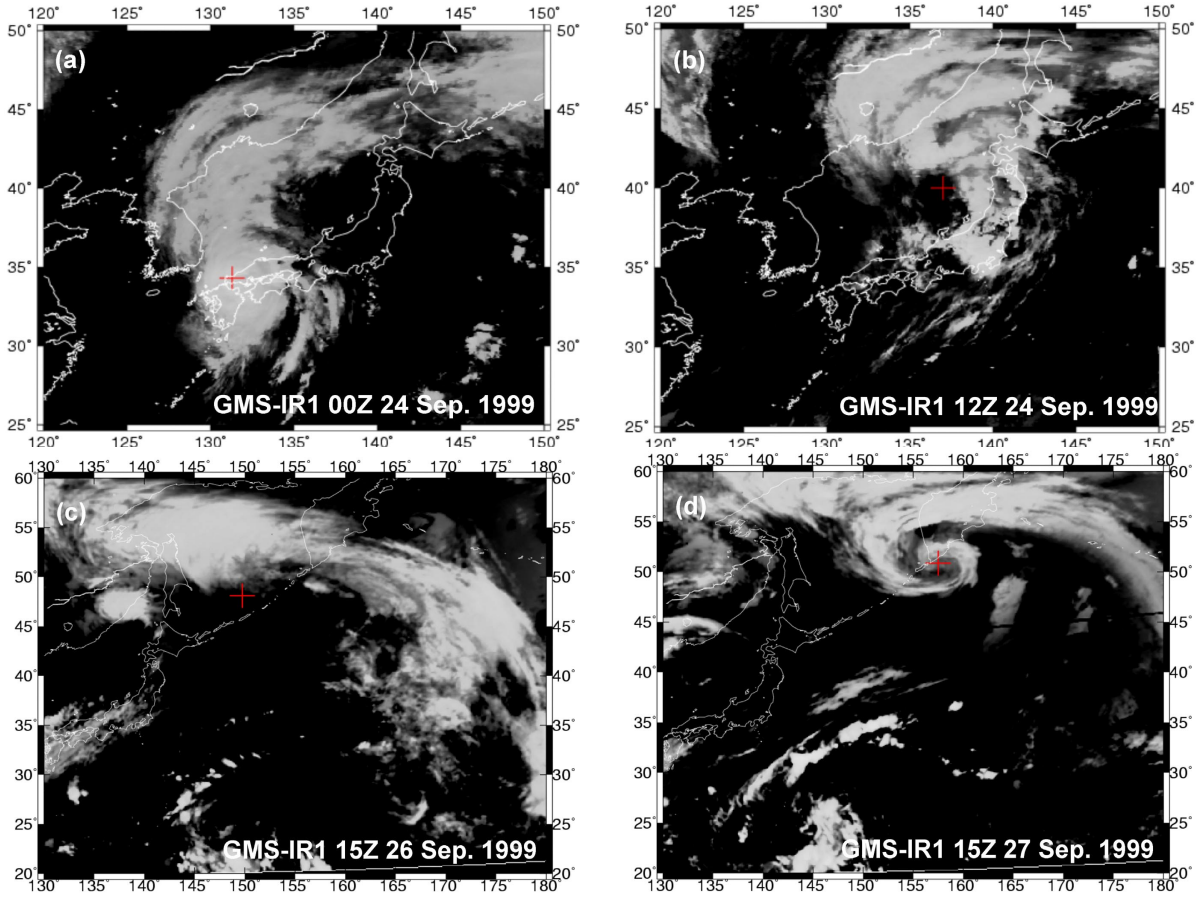

Figure 3 : GMS-5 infrared satellite images of Bart at 0000Z 24 September (mature stage (a)), 1200Z 24 (dissipating stage (b)), 1500Z 26 (weakest stage (c)), 1500Z 27 (re-intensified stage (d)). Plus signs in figures show the position of Bart's center reported in the JMA best track.

anomaly. The balance assumption made herein follows the Charney (1955) nonlinear balance equation:

$$\nabla^2\Phi = \nabla \cdot f\nabla\Psi + 2m^2\left[\frac{\partial^2\Psi}{\partial x^2}\frac{\partial^2\Psi}{\partial y^2} - \left(\frac{\partial^2\Psi}{\partial x\partial y}\right)\right] \quad (1)$$

where Φ is the geopotential, Ψ is the balanced wind stream function, and the other variables take on their usual meanings. The other diagnostic relation necessary for the inversion of Ψ and Φ is given by the following approximate form of the Ertel's PV definition:

$$\begin{aligned} q &= \frac{g\kappa\pi}{p}\left[(f + m^2\nabla^2\Psi)\frac{\partial\Phi}{\partial\pi^2}\right. \\ &- \left. m^2\left(\frac{\partial^2\Psi}{\partial x\partial\pi}\frac{\partial^2\Phi}{\partial x\partial\pi} + \frac{\partial^2\Psi}{\partial y\partial\pi}\frac{\partial^2\Phi}{\partial y\partial\pi}\right)\right] \quad (2) \end{aligned}$$

where q is the model-simulated Ertel's potential vorticity, and π is the Exner function. The form of closed system by (1) and (2) with appropriate boundary conditions is solved for the unknown Ψ and Φ given q (see Davis and Emanuel (1991) for details).

We consider that the PV anomaly field q' is partitioned into N portions of anomalies, $q' = \Sigma_{n=1}^{N} q_n$. Here, we adopt the linearized (1) and (2) for evaluations of the geopotential anomaly Φ_n and the stream function anomaly Ψ_n induced by each anomaly q_n. The resulting linear closed equations of the nth perturbation are:

$$\begin{aligned} \nabla^2\Phi_n = \nabla\cdot(f\nabla\Psi_n) + \\ 2\left(\frac{\partial^2\Psi_*}{\partial x^2}\frac{\partial^2\Psi_n}{\partial y^2} + \frac{\partial^2\Psi_*}{\partial y^2}\frac{\partial^2\Psi_n}{\partial x^2} - 2\frac{\partial^2\Psi_*}{\partial x\partial y}\frac{\partial^2\Psi_n}{\partial x\partial y}\right), \quad (3) \end{aligned}$$

and,

$$\begin{aligned} q_n &= \frac{g\kappa\pi}{p}\left[(f+\nabla\Psi_*)\frac{\partial^2\Phi_n}{\partial\pi^2} + \frac{\partial^2\Phi_*}{\partial\pi^2}\nabla^2\Psi_n\right. \\ &- \left(\frac{\partial^2\Psi_*}{\partial x\partial\pi}\frac{\partial^2\Phi_n}{\partial x\partial\pi} + \frac{\partial^2\Phi_*}{\partial x\partial\pi}\frac{\partial^2\Psi_n}{\partial x\partial\pi}\right) \\ &- \left.\left(\frac{\partial^2\Psi_*}{\partial y\partial\pi}\frac{\partial^2\Phi_n}{\partial y\partial\pi} + \frac{\partial^2\Phi_*}{\partial y\partial\pi}\frac{\partial^2\Psi_n}{\partial y\partial\pi}\right)\right], \quad (4) \end{aligned}$$

where $(\ )_* = \overline{(\ )} + \frac{1}{2}(\ )'$, and $\overline{(\ )}$ is the refrence state defined as a time average. The system (3)–(4) is solved for each PV anomaly using homogeneous boundary conditions for lateral boundaries, and Neumann boundary conditions for top and bottom boundaries. The next step is to partition the total PV anomaly q' into the distinct perturbations q_n of different origins. In this case, these are perturbations from the dry stratosphere depression ($\mathbf{Q_d}$), the surface baroclinicity ($\mathbf{Q}_\theta$), the wet tropopause depression associated with latent heat release ($\mathbf{Q_h}$), the negative PV anomalies ($\mathbf{Q_n}$), and the remnants ($\mathbf{Q_r}$).

5. RESULTS OF SIMULATED EXTRATROPICAL TRANSITION OF BART

The control simulation with the full physical processes successfully reproduces the realistic track and strength of Typhoon Bart. The MM5 simulates its rapid-decaying and re-intensifying stage of Bart, whereas the experiment could not capture its mature strength (a sea-level central pressure of 930-hPa) of Bart because of lack of the model resolution.

Figure 4 shows the MM5-simulated cloud distributions in (a) the weakest stage, 00Z 25 Sep., and (b) the re-intensified stage, 00Z 27 September. In the weakest stage, it should be noted that the simulated Bart possesses a significant asymmetric structure, in which the west-east-oriented cloud band formed at the north of the sea-level pressure minimum of Bart (see in Figure 4a). The feature is consistent with the GMS-5 observation as Figure 3 (c) shown. The asymmetry develops gradually as Bart approaches to the pre-existing synoptic system. However, it brings back its symmetric spiral cloud pattern, and decreases its sea-level central minimal pressure again (Figure 4 (b)). The simulated fields are in good agreement with the satellite-observed cloud pattern (Figure 3) and the JMA best track (Figure 1).

We shall now look more carefully into the re-intensifying stage of simulated Bart using a PV perspective. Figure 5 (a) shows a horizontal distribution of simulated PV at 10-km level, indicating that the high-PV air at this level is originating from the stratosphere. When Bart is in the re-intensifying stage over the Sea of Okhotsk, an upstream upper-level high PV anomaly is wrapped up cyclonically. The trough is vertically coupling with the low-level PV anomaly, which has its origin in the remnant of Bart in ET. The upstream perturbation was generated in the high-latitude stratosphere, and is intruded deeply into the mid-latitude troposphere. An upper-level negative PV anomaly relating to an upper-level outflowing jet stream is also located at the north of Bart and plays an important role in reinforcing the cyclonic activity, because the typhoon center is located at the right rear of the entrance of the upper-level jet streak. The negative PV anomaly and outflowing jet stream is prevailing, as a result of tropopause liftings and updrafts in the cloud band at the north of Bart, as the vertical cross section (Figure 5b) shown. Estimating each term in the vertical vorticity tendency equation, the strong vertical ascending results in the strong convergence of vertical vorticity at low-levels (not shown). As a consequence of the vorticity convergence, Bart is considered to be due to develop its cyclonic wrap-up again at mid-latitude (shown in Figure 6b). It is suggested that the re-intensification of Bart in mid-latitude is caused bythe followings; 1) the existence of the remnant of Bart which is containing the wet warm core structure, and 2) the upper-level upstream dry positive PV anomaly approaching to the typhoon center, and 3) the presence of the negative PV anomaly associated with the upper-level outflowing jet stream.

6. SENSITIVITY RESULTS OF EXTRATROPICAL TRANSITION OF BART

Several sensitivity experiments as well as the control simulation (hereafter CNTL) are examined on the rapid-decaying and re-intensifying stage of Bart in order to estimate the quantitative contributions of each physical process. The first sensitivity test is that the release of the latent heat of condensation is withheld (herein FDRY). The second experiment run without the boundary layer processes, latent heat flux and sensible heat flux (refered to as NOFLX). These experiments are initialized at 0000Z 24 September when Bart just begins its weakest stage.

Figure 6 (a) shows time series of the minimal sea-level pressure of Bart simulated by each sensitive experiment. The CNTL pressure fall is approximately -15 hPa during the weakest stage (990-hPa) to the re-intensified stage (975-hPa). The NOFLX experiment also reproduces its re-intensification (a pressure fall of -5-hPa), despite the pressure fall is quite small compared to CNTL. On the other hand, the effect of latent heat release in clouds on the cyclogenesis was considerable large, since the FDRY run exhibit almost no pressure fall in its re-intensifying stage. The contribution by latent heat release in clouds is more important than by boundary layer processes. These facts indicate that the boundary layer fluxes have little effect on the cyclogenesis of Bart in such a short time, and heating processes by condensation however have an important role in the rapid development.

Time series of vertical vorticity at low-levels (1.5-km AGL) in each sensitivity are also shown in Figure 6 (b). As Figure 6 (a) shown, the vertical vorticity at low-levels in CNTL and NOFLX increase to $0.0002 \sim 0.00025$ s^{-1} in the re-intensified stage. The difference of the maximum vorticity between CNTL and NOFLX is about 0.00005 s^{-1} at the re-intensified stage (at 06Z 26 Sep.). FDRY-simulated Bart however indicates no increase of its cyclonic activity. As described in previous section, it is obvious that the stretching generation of vorticity at low-levels due to strong up-

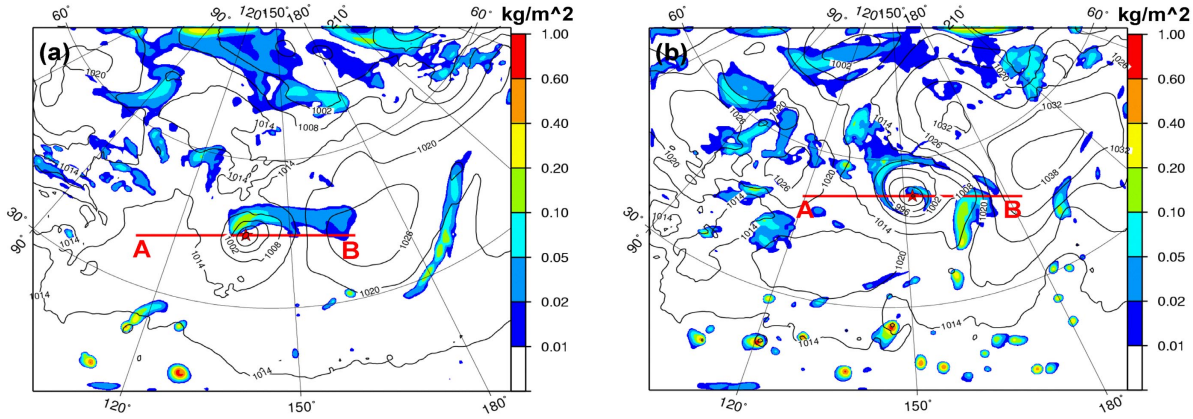

Figure 4 : Distributions of the MM5-simulated vertical integrated rain- and snow-water mixing ratio (shaded) and sea level pressure (contoured every 6 hPa) at (a) 0000Z 25 Sep. (weakest stage) and (b) 0000Z 27 Sep. (re-intensified stage). A star sign indicate the pressure minimal position on sea level.

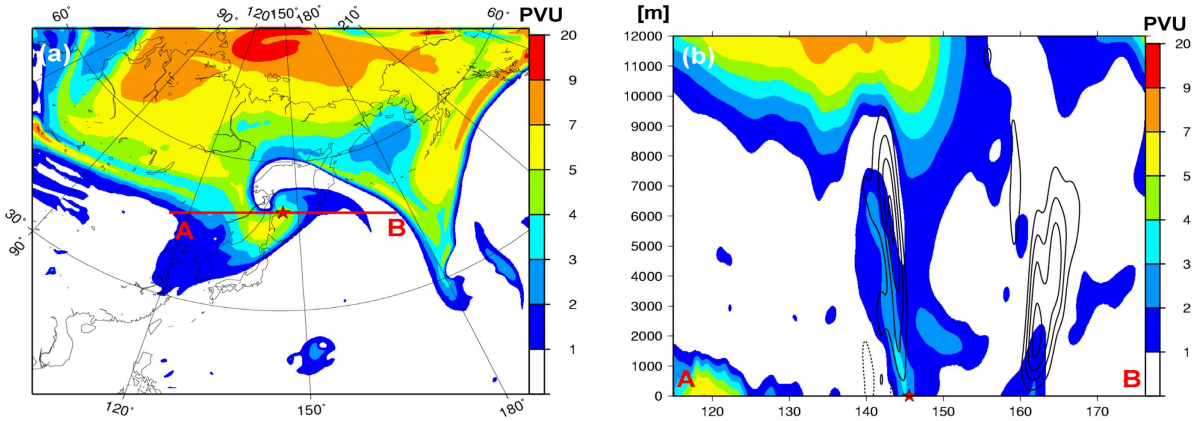

Figure 5 : (a) Horizontal distribution on 10-km levels and (b) A–B vertical cross section of the MM5-simulated PV field (shaded) at 0000Z 26 Sep. (in the process of re-intensifying). Contour lines in (b) imply the vertical velocity field every 5cm/sec. A star sign indicate the pressure minimal position on sea level.

drafts in clouds is quite important process for the re-cyclognesis.

The differences of flowing and PV between CNTL and FDRY (in the re-intensified stage) are shown in Figure 8. The large negative PV differences at upper-levels among these experiments ($PV_{cntl} - PV_{fdry} < 0$) are dominating over the north of Bart. The area is corresponding to the strong outflowing jet streak and the top of the intensive west-east-oriented cloud band in CNTL run. There are positive PV differences at low-levels in clouds ($PV_{cntl} - PV_{fdry} > 0$), as in Figure 7 (b), due to the lack of the latent heating in FDRY. Therefore, FDRY-simulated Bart is considered to be weakened because of suppressing the developments of low-level warm core and vorticity in clouds. As differential vectors at upper-levels ($\mathbf{U}_{cntl} - \mathbf{U}_{fdry}$) in Figure 7 (a) shown, the jet streak was approximately 10 m/s stronger in CNTL than in FDRY. The differential vectors at low-levels is prevailing around the warm conveyer belt to the east of the center (see in Figure 7 (b)). These results emphasize that the upper-level jet streak to the north of Bart can be strongly affected by the low-level condensation heating in its remnant.

7. ANALYSIS OF PIECEWISE PV INVERSION

We perform a piecewise PV inversion (described in section 4) on the rapid-decaying and re-intensification of Bart. Figure 8 shows that the estimated contributions of each PV anomaly to 1000-hPa geopotential height fall of the Bart's center. At 00Z 24 Sep. (in the mature stage), the $\mathbf{Q}_\mathbf{h}$ contribution is 84%, indicating that low-level warm core in Bart is most significant in all processes. In the decaying stage (during 00Z 24–12Z 25), the contribution of wet positive PV anomaly $\mathbf{Q}_\mathbf{h}$ is decreasing rapidly, and the contribution of boundary layer $\mathbf{Q}_\theta$ is increasing gradually. As

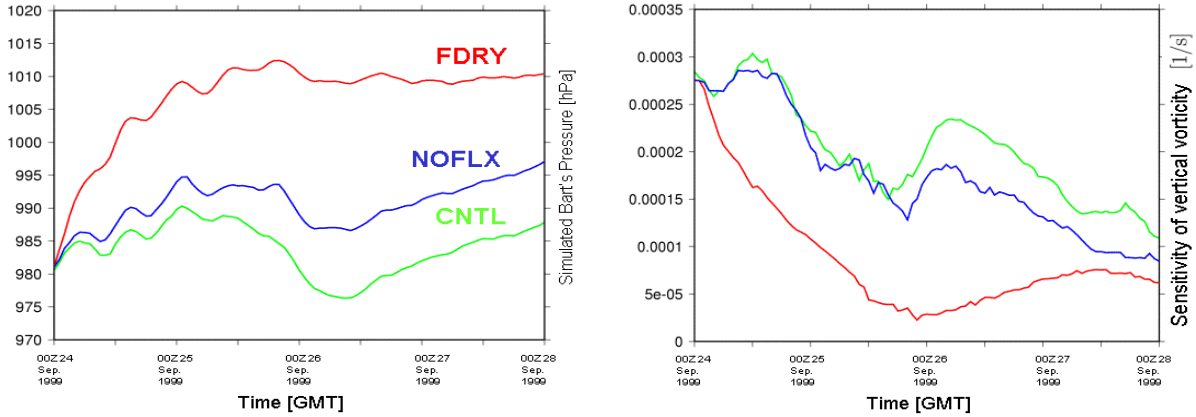

Figure 6 : Time series of (a) the minimal pressure on sea-level and (b) the positive maximum vertical vorticity on 1.5-km levels, around the MM5-simulated Bart in control run (CNTL; green line) and no-flux run (NOFLX; blue line) and fake-dry run (FDRY; red line).

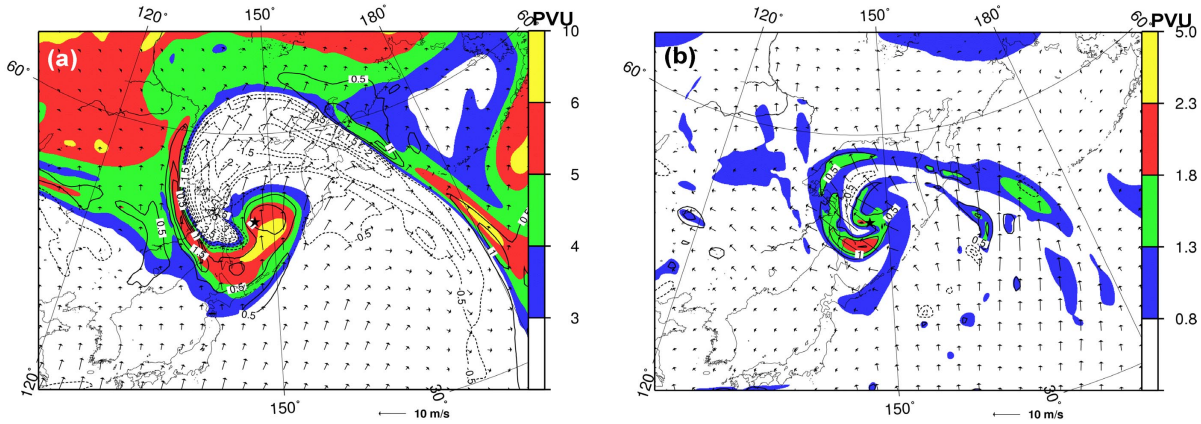

Figure 7 : Horizontal distributions of the MM5-simulated PV field (shaded) in CNTL on (a) 10-km level and (b) 5-km level, at 1200Z 26 September. $\mathrm{PV}_{cntl}-\mathrm{PV}_{fdry}$ field is shown by the solid (positive values) and dotted (negative values) lines, for every 0.5 PVU. Differential wind $\mathbf{U}_{cntl}-\mathbf{U}_{fdry}$ field are shown by the vectors. A star sign in figures indicate the pressure minimal position on sea level.

Bart approaches to the mid-latitude baroclinic zone, the negative PV anomaly $\mathbf{Q_n}$ contribution is increasing negatively ($-35\%\rightarrow-61\%$). In the weakest stage (12Z 25 Sep.), the $\mathbf{Q_n}$ contribution is -61% which is adversely comparable to the $\mathbf{Q_h}$ contribution (67%). It is suggested that the negative PV anomaly associated with the upper-level jet stream plays an important role in weakening the activity of the mid-latitudinal typhoon. However, the contribution of dry positive PV anomaly $\mathbf{Q_d}$ is increasing from 12% to 36% due to the approaching of the upper-level trough. During 12Z 25–12Z 26 (the re-intensifying stage), the $\mathbf{Q_n}$ ($\mathbf{Q_h}$) contribution is decreasing (increasing) gradually. On the other hand, the $\mathbf{Q_d}$ contribution is still increasing. In the re-intensified stage (at 12Z 26), the $\mathbf{Q_h}$ contribution (63%) is greater than the $\mathbf{Q_n}$ (-48$\%$). The upper-level dry trough effect $\mathbf{Q_d}$ accounts for about 50% of the total contributions, suggesting that the upper trough is coupling with the lower remnant ($\mathbf{Q_h}$). After the re-cyclogenesis (during 12Z 26–12Z 27), the increase of the negative PV anomaly $\mathbf{Q_n}$ contributes the central pressure raise, although the $\mathbf{Q_d}$ and $\mathbf{Q_h}$ contributions to cyclogenesis still carry on.

8. SUMMARY

In this study we performed a series of numerical experiments of the ET of Typhoon Bart using the PSU/NCAR MM5 (Dudhia 1993). The results simulated by MM5-CNTL were in good agreement with some observations. Especially, the weakening and re-intensifying stage of Bart could be successfully simulated.

When Bart in the re-intensifying stage moved into the synoptic baroclinic zone, Bart cyclonically wrapped

up the upper-level positive dry PV anomaly and accomplished to coupling with it vertically. Mid-latitudinal Bart was strongly influenced by both the upper-level outflowing jet streak and the low-level strong vertical motion in the remnant. A fake dry sensitivity experiment suggested that the outflowing jet was sustained by the latent heat release in the activated cloud bands. The point which the authors especially emphasize is that the re-intensification of Bart can be explained by the dynamic outflowing process (negative PV anomaly) at upper-levels and thermodynamic latent heating process (positive PV anomaly) at low-levels. However, the ET of TC might be not concluded by such a simple process only, because these PV anomalies interact with one another.

ACKNOWLEDGMENTS

The authors wish to thank the Japan Meteorological Agency and Japan Meteorological Business Support Center for providing some useful dataset (satellite image, typhoon best track) used in this study. Several helpful discussions with Dr. Y. Kurihara and Dr. Wang Zifa (Frontier Research System for Global Change, Kanagawa, Japan) are gratefully acknowledged. This study was funded by the JSPS research fellowships and the Grant-in-Aid for Scientific Research, the Ministry of Education, Culture, Sports, Science, and Technology.

REFERENCES

Bosart L. F, and G. M. Lackmann, 1995: Postlandfall tropical cyclone reintensification in a weakly baroclinic environment: A case study of hurricane David (September 1979). *Mon. Wea. Rev.*, **123**, 3268 – 3291.

Charney, J. G., 1955: The use of primitive equations of motion in numerical prediction. *Tellus*, **7**, 22 – 26.

Davis, C. A., and K. A. Emanuel, 1991: Potential vorticity diagnostics of cyclogenesis, *Mon. Wea. Rev.*, **119**, 1929 – 1953.

Dudhia. J, 1993: A nonhydrostatic version of the Penn State–NCAR Mesoscale Model: Validation tests and simulation of an Atlantic cyclone and cold front. *Mon. Wea. Rev.*, **121**, 1493 – 1513.

Low-Nam, S. and C. Davis, 2001: Development of a tropical cyclone bogussing scheme for the MM5 system. *Preprint for the Eleventh PSU/NCAR MM5 Users' Workshop*, Boulder, Colorado, 130 – 134.

McTaggart-Cowan, R., J. R. Gyakum, and M. K. Yau, 2001: Sensitivity testing of extratropical transitions using potential vorticity inversions to modify initial conditions : Hurricane Earl case study. *Mon. Wea. Rev.*, **129**, 1617 – 1636.

Ritchie, E. A. and R. L. Elsberry, 2001: Simulations of the transformation stage of the extratropical transition of tropical cyclones, *Mon. Wea. Rev.*, **129**, 1462 – 1480.

Sanders, F. and J. R. Gyakum, 1980: Synoptic-dynamic climatology of the "bomb"., *Mon. Wea. Rev.*, **108**, 1589 – 1606.

Thorncroft, C. and S. C. Jones, 2001: The extratropical transitions of hurricane Felix and Iris in 1995, *Mon. Wea. Rev.*, **128**, 947 – 972.

Thorncroft, C., B. J. Hosikins, and M. E. McIntyre, 1993: Two paradigms of baroclinic-wave life-cycle behaviour, *Quart. J. Roy. Meteor. Soc.*, **119**, 17 – 55.

Yoshino, J., H. Ishikawa, and H. Ueda, 2002: MM5 simulations of the 24 September 1999 tornadic outbreaks in the outer rainband associated with typhoon Bart, *Preprint for the twelfth PSU/NCAR MM5 Users' Workshop*, Boulder, Colorado, 86 – 89.

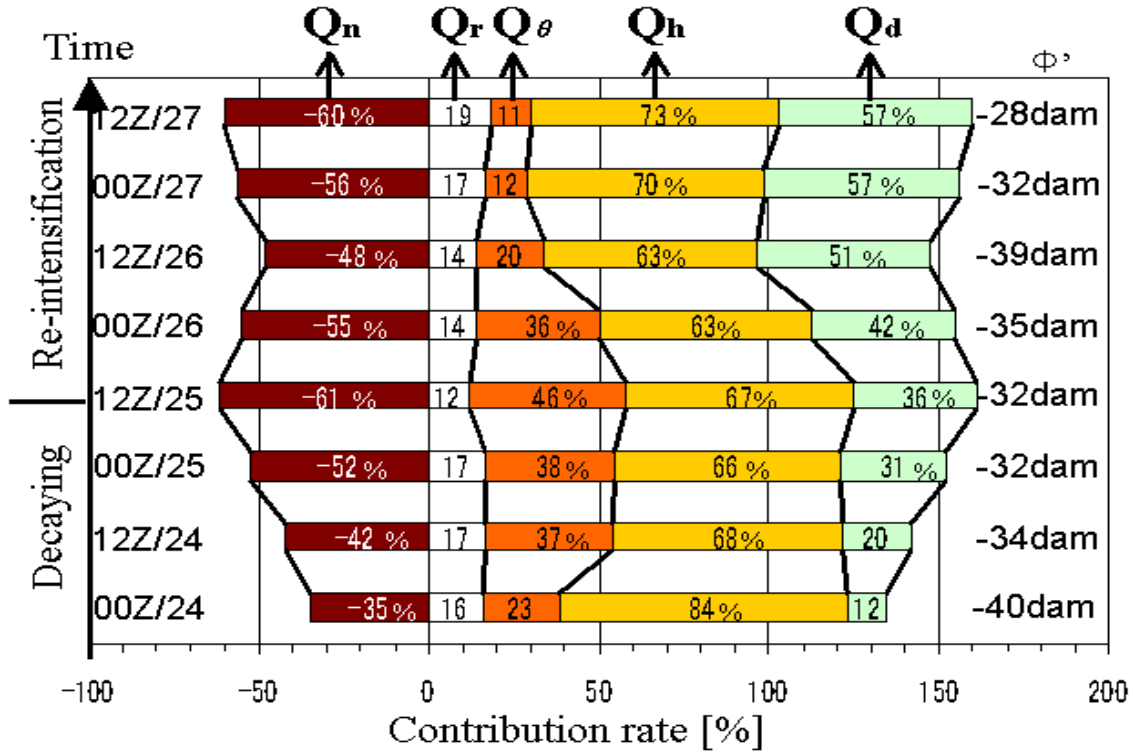

Figure 8 : The contributions to 1000-hPa geopotential height fall (dam) from the dry positive PV anomaly $\mathbf{Q_d}$, wet positive PV anomaly $\mathbf{Q_h}$, boundary layer $\mathbf{Q_\theta}$, negative PV anomaly $\mathbf{Q_n}$, and remnants $\mathbf{Q_r}$, during 00Z 24 – 12Z 27 September.